Asia-Pacific Journal of Science and Technology :Volume :30 Issue :05 Article ID :APST-30-05-06 Research Article

APST

Asia-Pacific Journal of Science and Technology

https//:www.tci-thaijo.org/index.php/APST/index

Published by Research and Innovation Department,
Khon Kaen University, Thailand

Andrographis paniculata extract, biochar, and g-C_3N_4 photocatalyst as functional fillers in alginate-based film for active packaging applications

Werachai Lipar[1], Orawan Chunhachart[2], Passorn Jongkaewvijit[2], Rudeerat Suntako[1], Wadchara Thongsamer[1], Warisa Singtakong[1], and Suntree Sangjan[1,*]

[1]Department of Physical and Material Sciences, Faculty of Liberal Arts and Science, Kasetsart University Kamphaeng Saen campus, Nakhon Pathom, 73140, Thailand
[2]Division of Microbiology, Department of Science and Bioinnovation, Faculty of Liberal Arts and Science, Kasetsart University Kamphaeng Sane Campus. Nakhon Pathom, 73140 Thailand
*Corresponding author: faasstp@ku.ac.th

Received 10 September 2024
Revised 27 February 2025
Accepted 6 May 2025

Abstract

Plastic films, widely used in food packaging, pose a particular challenge due to their non-biodegradability. This study explores the development of biodegradable and eco-friendly packaging films using sodium alginate as the base polymer, enhanced with *Andrographis paniculata* herbal extract, biochar, and graphitic carbon nitride (g-C_3N_4) nanosheets. The process involved extracting *A. paniculata* using microwave and ultrasonic treatments, synthesising biochar from *Grammatophyllum specinocum BL* branches through pyrolysis, and creating g-C_3N_4 nanosheets from urea. Composite films were prepared by blending these additives with sodium alginate and glycerol, followed by ultrasonic processing and thermal drying. The films' properties were characterised using fourier transform infrared spectroscopy (FTIR), scanning electron microscopy (SEM), and mechanical testing. The mechanical testing results reveal that biochar significantly improved the film's modulus, indicating enhanced strength and rigidity, whereas herbal extracts increased the film's elongation but reduced its modulus. Microstructures showed uniform distribution of biochar particles and aggregation of g-C_3N_4, which influenced the film's surface properties. Composite films with *A. paniculata* extract, biochar, and g-C_3N_4 exhibited the highest contact angles, indicating hydrophobicity surface, and reduced water swelling compared to the control film. Additionally, the antioxidant activity of films containing herbal extracts was significantly enhanced. Finally, it was found that the alginate film enhanced with biochar, herbal extracts, and g-C_3N_4 photocatalyst significantly improved its properties and increased its potential for use as active packaging.

Keywords: *Andrographis paniculata*, Biochar, Photocatalyst, Active packaging, Antioxidant

1. Introduction

In the past decade, global production of plastic has exceeded 359 million tons annually, leading to a significant plastic waste issue. Research indicates that only about 25% of this plastic waste is recyclable. Most of the remaining waste consists of single-use plastics, exacerbating the environmental challenge [1]. Currently, plastic films are extensively used for food packaging, leading to a continuous increase in plastic waste.

These films, made from various petrochemicals such as low-density polyethylene (LDPE), linear low-density polyethylene (LLDPE), ethylene vinyl acetate (EVA), and polyvinyl chloride (PVC) are designed to wrap and preserve food. Their widespread use spans both household and industrial sectors due to their strength, tear resistance, and cost-effectiveness. However, plastic films are single-use items and cannot be reused, leading to significant waste accumulation. Like other plastics, these films take a long time to decompose naturally and pose long-term environmental risks if not properly managed. To address this issue, there are ongoing efforts to develop alternative materials derived from natural sources that are biodegradable and environmentally friendly. Promising substitutes include alginate, chitosan, polyvinyl alcohol, and cellulose, which aim to replace petrochemical-based

films. Alginate is a biodegradable polymer that is non-toxic, inexpensive, and biocompatible. It has been utilised in various fields, including biomedical materials, food packaging, and agriculture. Despite its advantages, alginate films have low mechanical strength, antioxidant, and antimicrobial properties. This limits their effectiveness in certain applications compared to traditional plastic films.

Andrographis paniculata is an annual plant characterised by its square stem and numerous branches. All parts of the plant have a bitter taste. The branches bear square-shaped leaves. This plant is commonly found in Thailand, Laos, Cambodia, Malaysia, Indonesia, Vietnam, China, and various Caribbean islands. Research indicates that *A. paniculata* extract contains compounds from the diterpene and flavonoid including andrographolide, deoxy andrographolide, neo andrographolide, methyl wogonin, apigenin, and onysilin [2-4]. Poushali Saha et al. demonstrated that natural diterpenes and diterpenoids possess significant antibacterial and antioxidant properties [5]. Flavonoids are a group of natural compounds with diverse phenolic structures found in fruits, vegetables, and herbs [6]. Today, they are considered essential components in nutraceuticals, pharmaceuticals, and cosmetics, largely due to their antioxidant, anti-inflammatory, anti-mutagenic, and anti-cancer properties [7]. Biochar is a carbon-structured material derived from biomass, such as agricultural waste including branches, tree bark, rice straw, and corn cobs, through a pyrolysis process. Currently, biochar is used as an additive in plastic packaging to enhance various properties, such as thermal stability, chemical inertness, biosensing capabilities, and active packaging materials [8]. Adding biochar to polymer films can enhance their strength, which addresses the relatively low mechanical strength of alginate films. Biochar particles improve the mechanical properties and thermal stability of these films, making them more suitable for various applications. Seth Kane et al. investigated the effects of incorporating biochar into recycled plastics and discovered that adding 40% biochar resulted in a 45% increase in tensile strength, a 126% improvement in stiffness, and a 79% enhancement in flexural storage modulus [9]. Similarly, Mariem Zouari et al. reported that introducing 5 wt% biochar into polylactic acid (PLA) and hemp-PLA composites notably boosted their tensile strength and elasticity [10]. g-C_3N_4 is an organic photocatalyst with a nanosheet structure like graphene. Its chemical structure comprises a triazine ring (C_3N_3) and a 3-s-triazine ring (C_6N_7). g-C_3N_4 is non-toxic, easily synthesised, cost-effective, and possesses antimicrobial properties, making it a versatile material for various applications [11]. Rui Li et al. reported that g-C_3N_4 nanosheets incorporated into polyacrylonitrile (PAN) functionalised composite membranes exhibit strong antibacterial activity [12].

The present study seeks to contribute to the development of innovative packaging films that prioritise environmental sustainability. The approach involves incorporating alginate polymer alongside biochar synthesised from agricultural waste, aiming to create a biodegradable and eco-friendly packaging solution. Additionally, the inclusion of *A. paniculata* herbal extract and g-C_3N_4 photocatalyst to load in the composite films. These additives are intended to reduce the oxidation process and inhibit the growth of pathogenic microorganisms in food, further enhancing safety of long-life shelf food.

2. Materials and methods

2.1 Extraction of herbs from Andrographis paniculata

Andrographis paniculata leaves were dried and ground into a fine powder which was then sieved through a 60-mesh sieve. Next, 1 g of *A. paniculata* powder was added to 100 mL of distilled water, then put it through a microwave at 800 watts for 2 min, before being filtered to remove the solids. After that, it was passed through an ultrasonic probe for 5 min. The final step was to filter it with a 0.22 µm syringe filter to obtain an *A. paniculata* herbal extract.

2.2 Biochar synthesis from Grammatophyllum specinocum BL

Grammatophyllum specinocum BL branches were burned under a pyrolysis process at 550°C for 2 hours, after which the biochar was ground into a fine powder. The material was then sieved with a 60-mesh sieve. The next step was to stimulate the biochar using a microwave. One gram of biochar was added to 100 mL of distilled water and subjected to microwave treatment at 800 watts for 2 min, followed by filtration. The solids were removed by centrifuging the substance at 5000 rpm for 30 seconds. The precipitate was then filtered out and the clear part was passed through an ultrasonic probe for 5 min, after which it was filtered with a 0.22 µm syringe filter. The final product is a biochar solution, ready for use to enhance the properties of biodegradable packaging films. This process ensures the biochar is finely processed and activated, optimising its effectiveness in improving thermal stability and mechanical properties.

2.3 Synthesis of g-C_3N_4 nanosheets

The synthesis of g-C_3N_4 nanosheets typically followed a thermal polymerisation method using nitrogen-rich precursors. In this research, urea was used as the precursor. 10 g of urea was placed in a crucible and burned at 550°C for 4 hours to obtain a g-C_3N_4 nanosheet powder.

2.4 Preparation of control film and alginate-based composite films

2.4.1 Preparation of control film

0.7 g of sodium alginate and 0.21 g of glycerol added to 50 mL of distilled water, stirred until a homogeneous state, passed through an ultrasonic bath at a temperature of 80°C for 30 min, passed through an ultrasonic probe for 5 min, and then poured into a glass petri dish. After that, it was baked with hot air at a temperature of 80 °C for 24 hours.

2.4.2 Preparation of alginate-based composite films

0.7 g of sodium alginate and 0.21 g of glycerol were added to 50 mL of distilled water and stirred until a uniform mixture was obtained. After that, the biochar solution, *A. paniculata* extract, and g-C_3N_4 were added, as shown in Table 1. After that, they were stirred to a homogeneous state and then passed through an ultrasonic probe for 5 min, before being poured into a glass petri dish and baked at 80°C for 24 hours.

Table 1 Components of control film and alginate-based composite films.

Sample	SA (g)	Biochar (mL)	Herb extract (mL)	g-C_3N_4 (g)
Control film	0.7			
AB	0.7	10		
AG	0.7			0.007
AH	0.7		10	
AHB	0.7	10	10	
AHG	0.7		10	0.007
ABG	0.7	10		0.007
ABHG	0.7	10	10	0.007

2.5 Characterisation

2.5.1 Morphology

The crystal structure, chemical structure, and morphology were analysed using various processes, namely Fourier Transform Infrared Spectroscopy (FTIR), X-Ray Diffractometer (XRD), and Scanning Electron Microscope (SEM).

2.5.2 Mechanical properties

The mechanical properties were studied with a universal testing machine by cutting a film sample of size 6 cm x 1cm. The speed of the fixation point was set at 40 mm/min. Each sample was measured three times.

2.5.3 Water solubility

The water swelling value of a film indicates its ability to resist water diffusion into the film. The film was baked at 60°C for 24 hours to find the dry weight (W_{dry}). After that, it was soaked in distilled water for 2 hours and weighed to give the wet weight (W_{wet}). The water swelling value of the film was then calculated from the following equation [13].

$$Swelling(\%) = \left(\frac{W_{wet} - W_{dry}}{W_{dry}}\right) \times 100 \quad (3)$$

2.6 Antioxidant activity

Antioxidant activity was examined using the DPPH radical scavenging assay. A solution of 1, 1- diphenyl-2-picryhydrazly (DPPH) with a concentration of 0.1 mM in ethanol was prepared and stored in the dark. 1 mL of the sample solution was taken and then 1 mL of DPPH was added before keeping it in the dark for 30 min, and then the absorbance was measured at a wavelength of 517 nm. The DPPH radical scavenging activity (%) was calculated using the following equation.

$$\%DPPH\ radical\ scavenging\ activity(\%) = \left(\frac{A_{DPPH} - A_{Sample}}{A_{DPPH}}\right) \times 100 \quad (4)$$

where A_{DPPH} and A_{Sample} are the absorbance values of DPPH solution and sample solution, respectively.

3. Results and discussions

Our research utilises g-C_3N_4 as an additive in active packaging to enhance antimicrobial performance. Anbarteh R. et al. demonstrated that g-C_3N_4 effectively inhibits bacterial growth, particularly against Staphylococcus aureus (*S. aureus*) and Escherichia coli (*E. coli*) [14]. The study of the chemical bond structure of g-C_3N_4 nanosheets using FTIR spectroscopy (Figure 1(A)) revealed specific bond vibrations, including tri-s-triazine cycles at a wave number of 810 cm, C-N bond vibrations at 1237, 1318, and 1407 cm, and C=N bond vibrations at 1455, 1552, and 1630 cm. These experimental results confirm that the g-C_3N_4 nanosheets are composed entirely of covalently linked, sp^2-hybridized carbon and nitrogen atoms [15,16].

In addition, the pseudo-second-order reaction rate for the degradation of Methylene blue (MB) was calculated by adding 0.2 g of g-C_3N_4 nanosheets to 100 mL of MB solution (10 ppm), collecting 0.5 mL of the MB solution every 20 min for 4 hours, and measuring the absorbance at 665 nm. After that, it can be used to calculate the efficiency of photodegradation as shown Figure 1(B) (inset). The results indicate that g-C_3N_4 nanosheets successfully removed about 55.17% of the MB dye within 4 hours. In addition, the pseudo second order reaction rate was studied as shown Figure 1(B). For a pseudo second order reaction, the rate law is given by the following equation [17]

$$\frac{t}{q_t} = \frac{1}{(kq_e^2)} + \frac{t}{q_e} \quad (1)$$

where k is the pseudo-second-order rate constant (g/m.hr), q_e is the amount of MB sorbed at equilibrium (mg/g), and q_t is amount of MB on the surface at any time, t.

From the pseudo-second-order kinetics graphs, the pseudo-second-order rate constant can be obtained from the y-intercept of the graph, while the equilibrium adsorption capacity (q_e) can be determined from the reciprocal of the slope. The results show that the pseudo second order reaction rate of g-C_3N_4 nanosheets was 1.98 g/(g.hr) and the absorption capacity at equilibrium was 5.26 mg/g. In addition, our previous study suggests that g-C_3N_4 nanosheets have an energy gap of 2.75 eV, enabling them to function effectively in the visible light range [18].

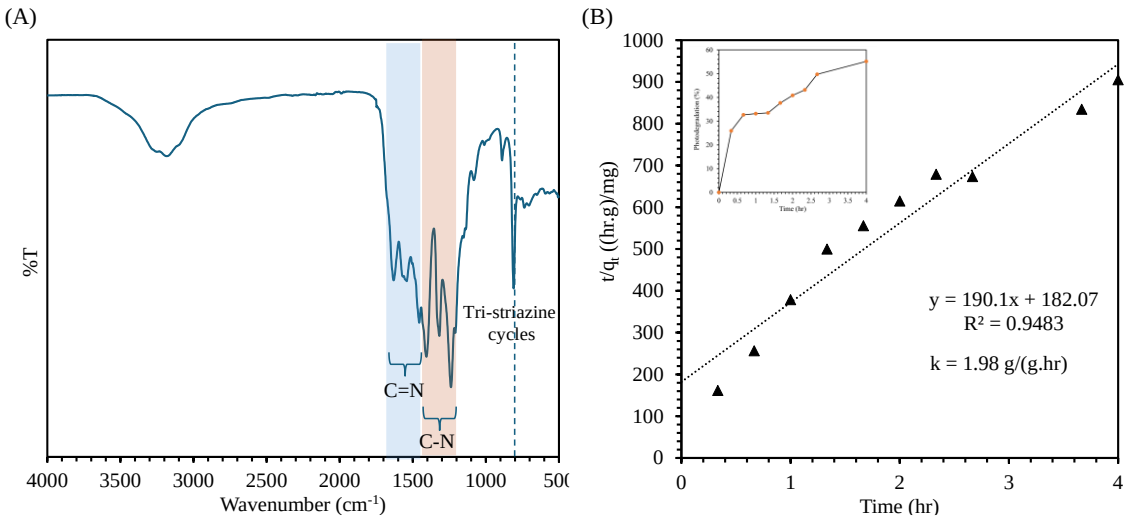

Figure 1 FTIR spectrum (A) kinetics graphs of pseudo-second order and (inset) MB removal photodegradation (B) of g-C_3N_4 nanosheets.

Antimicrobial of g-C_3N_4 nanosheets was determined by poison food technique using personal digital assistants (PDA) mixed with 1.0% (w/v) of g-C_3N_4, *Fusarium* sp. cultured on PDA for 7 days were used in this experiment. PDA was used as a negative control and PDA supplemented with 0.5% (w/v) of Metalaxyl was used as a positive control. Then the fungal hyphae were punched by using Cork borer with 0.7 cm in diameter. The fungal hyphae were placed on the surface of PDA and the plates were incubated at 35±2 °C for 7 days. The percentage of inhibition was calculated as described by Erhonyota et al. [19] using the following equation.

$$Percentage\ of\ inhibition\ (\%) = \frac{(C - T)}{C} \times 100 \quad (2)$$

where, C is the diameter of the colony on the negative control plate and T is the diameter of the colony on the plate supplement with composites.

The antifungal efficacy of 1.0% g-C_3N_4 against Fusarium sp. was demonstrated by a percentage inhibition of 21.12±0.60, which surpasses the inhibition observed with 0.5% Metalaxyl (16.70±1.25) as shown in Figure 2. Materials with a two-dimensional structure, such as g-C_3N_4, often possess sharp edges that can physically disrupt microbial cells, leading to cellular dysfunction and leakage of cytoplasmic contents due to damage to cell walls and membranes. Additionally, other reported mechanisms include the internalisation and transport of metal ions into microbial cells, which can impair intracellular ATP synthesis and interfere with DNA replication [20].

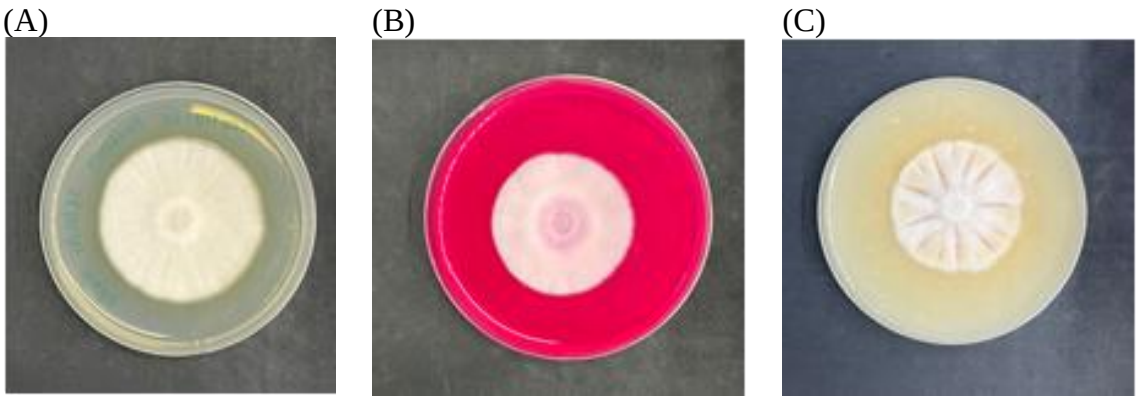

Figure 2 Antifungal activity of (A) negative control, (B) 0.5% Metalaxyl and (C) 1.0% g-C_3N_4 against *Fusarium* sp.

The chemical bonding structure of the alginate film (control film) and alginate-based composite film is shown in Figure 3. It was found that the control film exhibits 3280 cm, which correspond to the primary-secondary amines compounds. The vibrational peaks at 1597 and 1421 cm correspond to the C-C stretch in aromatic. The vibrations at peaks 1119, 1081, and 1000 cm correspond to the C-O stretch bond structure in the carboxyl group functional group. The vibrations at positions 936 and 807 cm correspond to the C-H stretch bond structure in aromatic. These observed chemical bond structures are consistent with the known structure of alginate, confirming the integrity and expected composition of the alginate control film. In addition to the observed peaks in the control film, the alginate composite films with added g-C_3N_4 exhibited additional vibrational peaks at 1317 and 1238 cm, which corresponded to the C-N stretch bond structure that appears in aromatic amines. The appearance of these additional peaks confirms the incorporation and presence of g-C_3N_4 in the composite films.

This analysis verifies that the g-C_3N_4 structure has been successfully integrated into the alginate matrix, enhancing the composite film's properties. When biochar molecules and *A. paniculata* extract were added to the composite film, no distinct changes in the chemical bond structure were observed compared to the control alginate film. Mengxiong Wu et al. [21] analysed the chemical bond structure of biochar and identified carbonyl, hydroxyl, and aliphatic C−H groups, with vibrational peaks appearing in the 700–900 cm range. In the case of *A. paniculata* extract, the main structures were found to be aromatic amines, aromatics, and amines, with vibrational peaks observed at approximately 1402, 1651, and 3286 cm^{-}, respectively [22]. The fact that the chemical bond structure does not change may be attributed to the overlapping chemical bonds within the biochar and herbal extract with those already present in the alginate film. Despite the addition of these components, the chemical bond structures detected via FTIR remained consistent with those of the alginate film. This suggests that the biochar and *A. paniculata* extract did not introduce new or distinguishable chemical bonds within the detection limits of the FTIR

analysis. The functional groups in the added substances likely share similar vibrational frequencies with those in the alginate, leading to overlapping peaks.

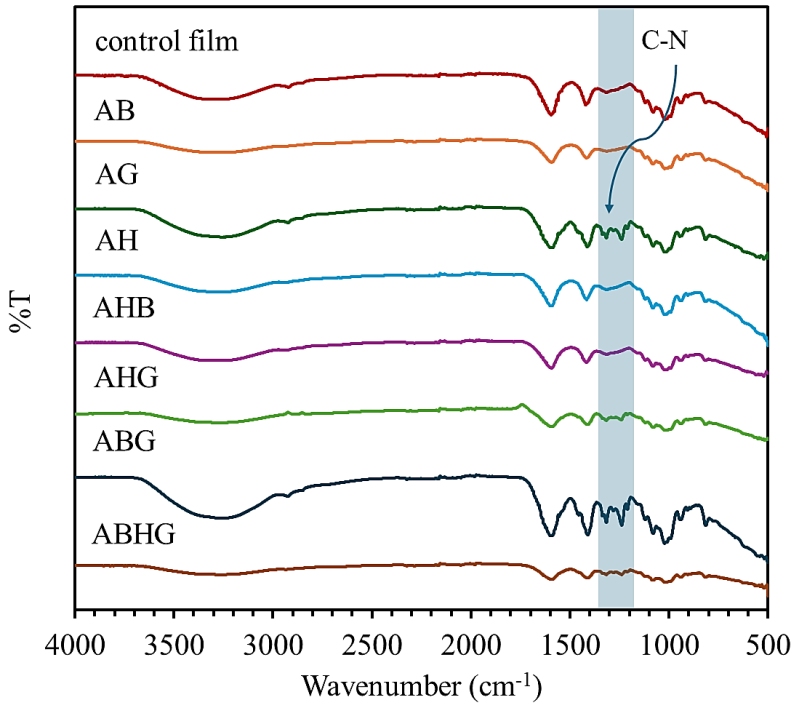

Figure 3 FTIR spectra of the control film and alginate-based composite films.

The crystal structures of alginate films and alginate composite films were analysed using XRD, as shown in Figure 4. The results reveal that alginate films incorporating *A. paniculata* extract exhibited diffraction peaks at 20.9° and 21.2°. This can be attributed to the presence of phenolic compounds in the extract, which induce structural modifications in the alginate matrix. The oxidation reaction between hydrogen bonds and phenolic acids enhances the organisation of alginate chains and increases crystallinity [23].

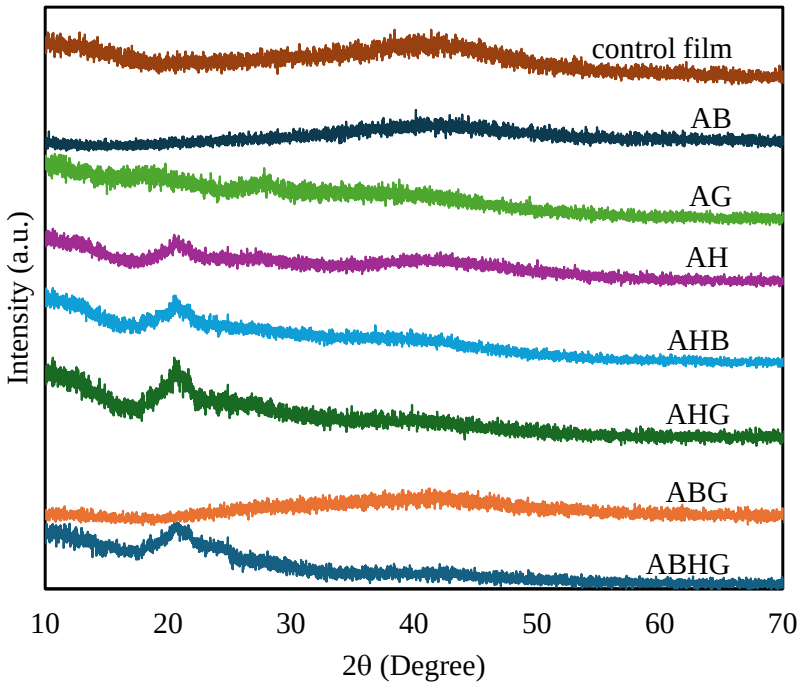

Figure 4 XRD pattern of control film and alginate-based composite films.

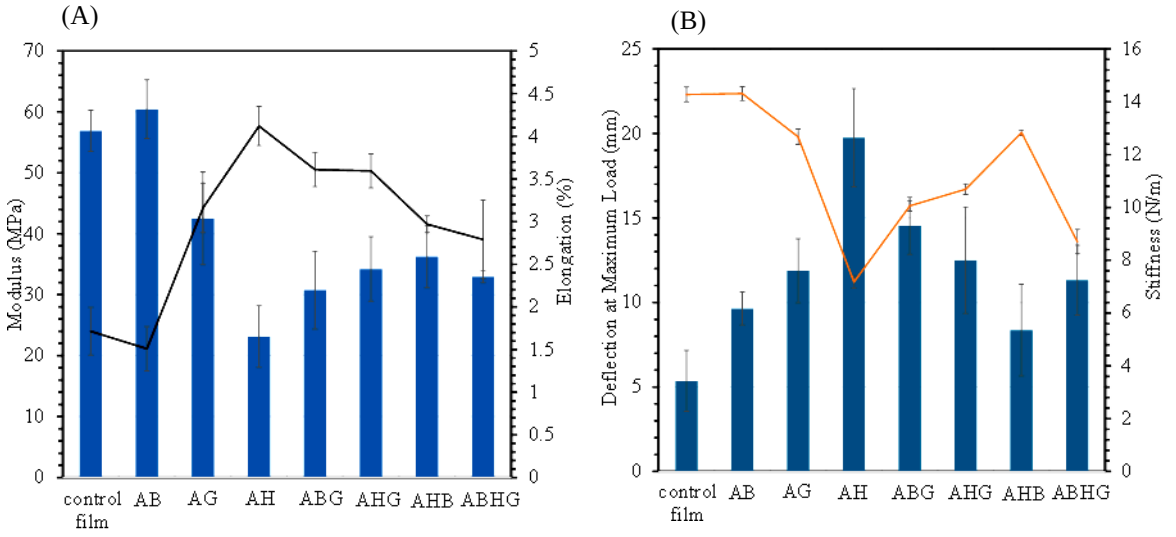

Figure 5 Mechanical properties: (A) the modulus (blue bars) and elongation at break (black line), and (B) deflection at maximum load (blue bars) and stiffness (orange line) of control film and alginate-based composite films

Figure 5(A) illustrates the modulus and elongation values of the control alginate film and the alginate-based composite films. The results reveal significant differences in the mechanical properties based on the additives used. The alginate composite film with added biochar, AB film, exhibited the highest modulus value. The addition of biochar to alginate films substantially improves their modulus, indicating increased strength and rigidity. The incorporation of biochar, a material with a strong carbon structure, significantly enhances the mechanical strength of the alginate composite film. The carbon framework of biochar increases the rigidity and resistance to deformation, resulting in a higher modulus. These results confirm that biochar is a valuable additive for strengthening alginate composite films. Further studies may focus on optimising the balance between strength and flexibility for specific packaging applications.

In contrast, the alginate composite film with added herbal (*A. paniculata*) extracts, AH film, showed the lowest modulus value and the highest elongation value. We expect that the herbal extracts contain phenolic compounds and flavonoids, which have hydroxyl groups in their structures. These hydroxyl groups can interfere with the alginate film's organic structure, potentially disrupting its integrity. This interaction can weaken the film, leading to a significant decrease in its modulus value. Consistent with the research of Mohamed S. Abdel Aziz et al., it was found that the addition of garlic oil extract, primarily composed of flavonoids, into the alginate film resulted in a reduction of the film's tensile strength [24]. However, according to the experimental findings, the film exhibited the highest stretch when herbal extracts were added, whereas the addition of biochar resulted in the lowest stretch. This observation can be attributed to the destruction of the film's internal bonding structure, which typically leads to increased softness and higher tensile strength. Also, the experimental results indicated that incorporating biochar enhanced the strength of the AB film. In contrast, the addition of *A. paniculata* extract reduced the strength of the AH film. This reduction may be attributed to the phytochemicals in *A. paniculata*, such as flavonoids and phenolic compounds, which act as reducing agents and disrupt the alginate network, weakening the film structure. The decrease in strength observed in AG films is likely due to the inhomogeneous aggregation of g-C_3N_4 and alginate, leading to structural defects. In ABHG films, which contain biochar, *A. paniculata* extract, and g-C_3N_4, the strength was lower than that of AB films but remained higher than that of AH films. These presented results underscore the balance between strength and flexibility when integrating various additives. This highlights the importance of meticulously selecting and optimising components during the development of composite films.

Figure 5(B) illustrates the deflection and stiffness values of both the control film and composite alginate films. It was observed that the alginate film with herbal extracts added exhibited the highest softness value, whereas the control film demonstrated the lowest deflection value. This suggests that the addition of herbal extracts enhances the flexibility of the films. Conversely, films with herbal extracts also showed the lowest hardness values. This phenomenon may be attributed to the nature of g-C_3N_4 as an n-type semiconductor, which exhibits a negative surface charge like alginate, an anionic polysaccharide. This similarity in charge characteristics can lead to the aggregation of g-C_3N_4 particles. In contrast, such aggregation is less likely to occur with nano-biochar due to electrical repulsion, resulting in a more homogeneous surface condition.

From the analysis of surface conditions depicted in Figure 6(A), the surface of the alginate film (Control film) is smooth and homogeneous. It was observed that incorporating nano-biochar into the alginate films resulted in a

uniform distribution of nano-biochar particles (Figure 6(B)), whereas the addition of g-C_3N_4 led to the aggregation of g-C_3N_4 particles (Figure 6(C)). For the films containing herbal extracts (AH) as shown in Figure 6(D), surface defects were observed, which may be attributed to the impact of phenolic acids present in the extracts. Regarding the addition of herbal extracts, it was observed that the surface condition of the alginate film underwent slight changes. This can be attributed to the flavonoid composition of the extract, which contains hydroxyl functional groups. These groups can release H+ ions, leading to the disruption of certain surface structures. However, it was observed that the addition of herbal extracts had a comparatively minor effect on altering the surface condition of the film, unlike the significant impact seen with the addition of g-C_3N_4 and biochar. This highlights that the presence of g-C_3N_4 and biochar induces substantial changes in the surface condition of the alginate film.

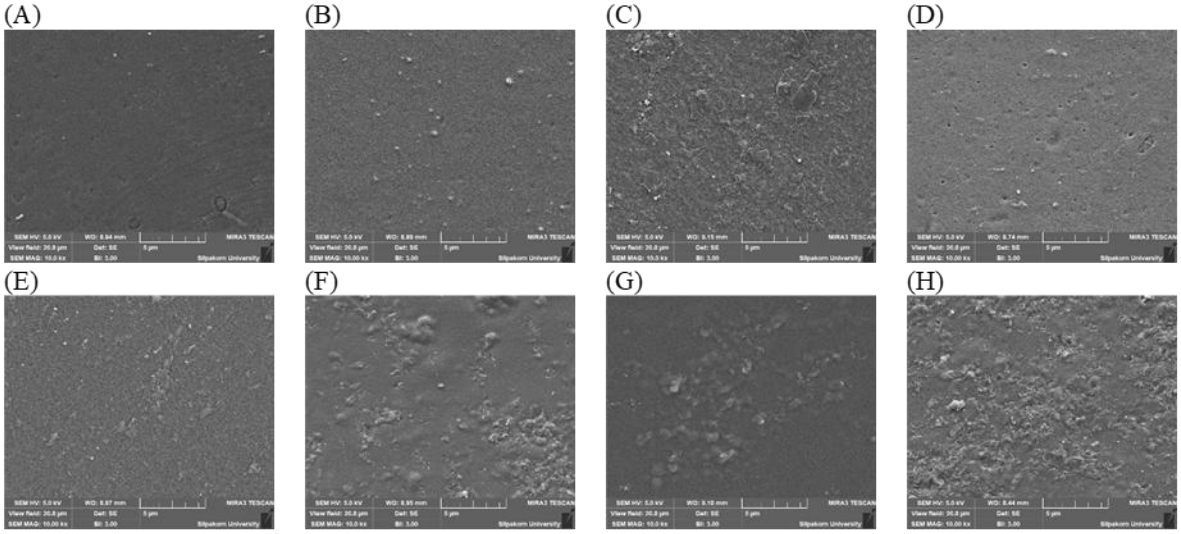

Figure 6 SEM images of (A) the control film and the alginate-based composite films: (B) AB, (C) AG, (D) AH, (E) AHB, (F) AHG, (G) ABG and (H) ABHG.

From the analysis of the overall surface condition of alginate-based composite films, it was found that the primary factor contributing to increased surface roughness was the addition of g-C_3N_4. In contrast, the addition of biochar and herbal milling agents caused only slight changes in the surface conditions.

The EDS spectrum of control film and alginate-based composite films clearly shows the presence of corresponding elements in its chemical structure (Figure 7A-H). Each spectrum shows characteristic peaks corresponding to elements present within the films, revealing insights into the chemical components and the effect of each additive.

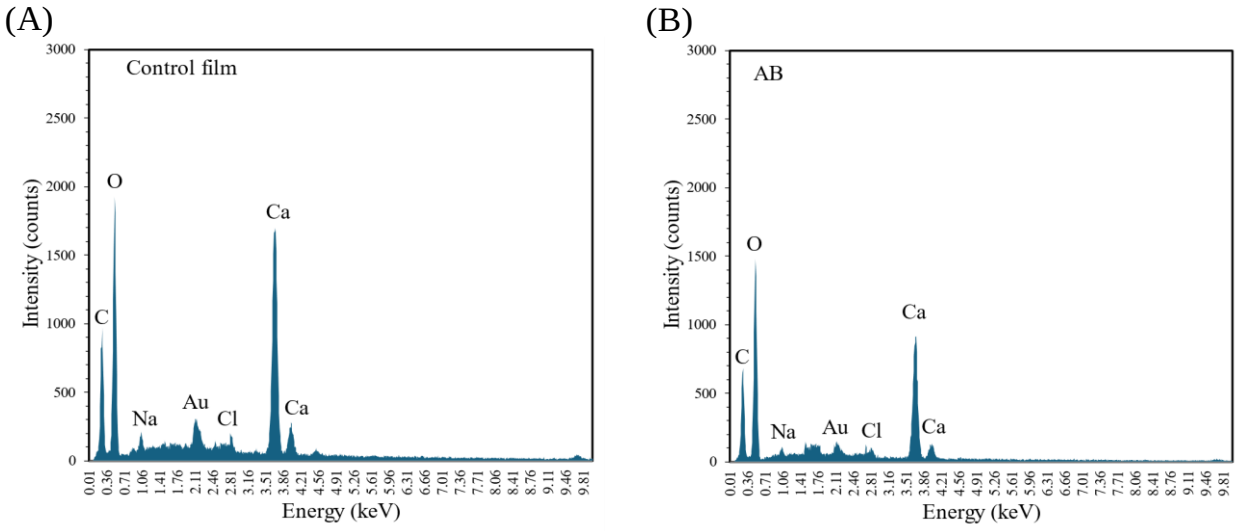

Figure 7 EDS spectrum of (A)control film and the alginate-based composite films: (B) AB, (C) AG, (D) AH, (E) AHB, (F) AHG, (G) ABG and (H) ABHG.

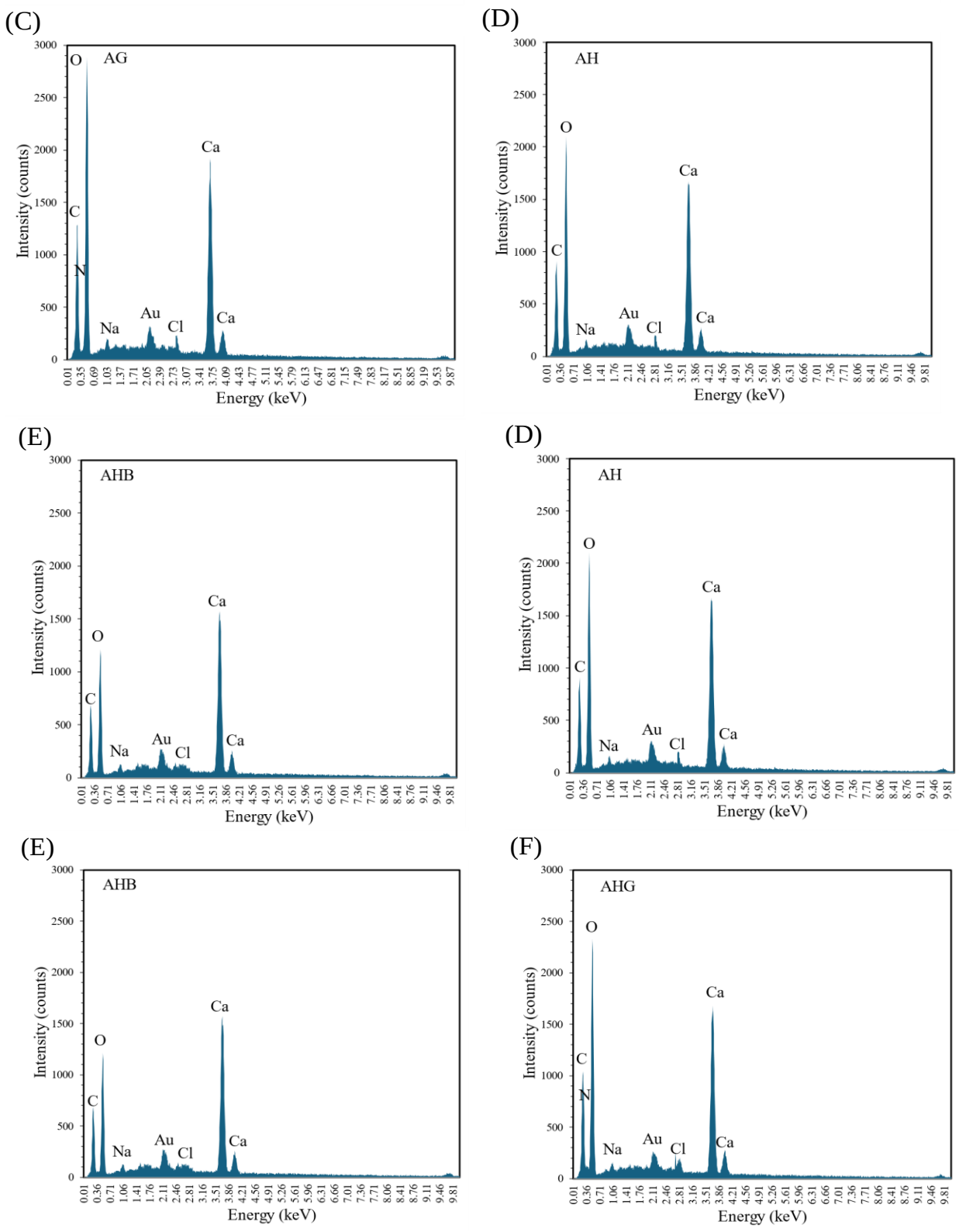

Figure 7 (Cont.) EDS spectrum of (A)control film and the alginate-based composite films: (B) AB, (C) AG, (D) AH, (E) AHB, (F) AHG, (G) ABG and (H) ABHG.

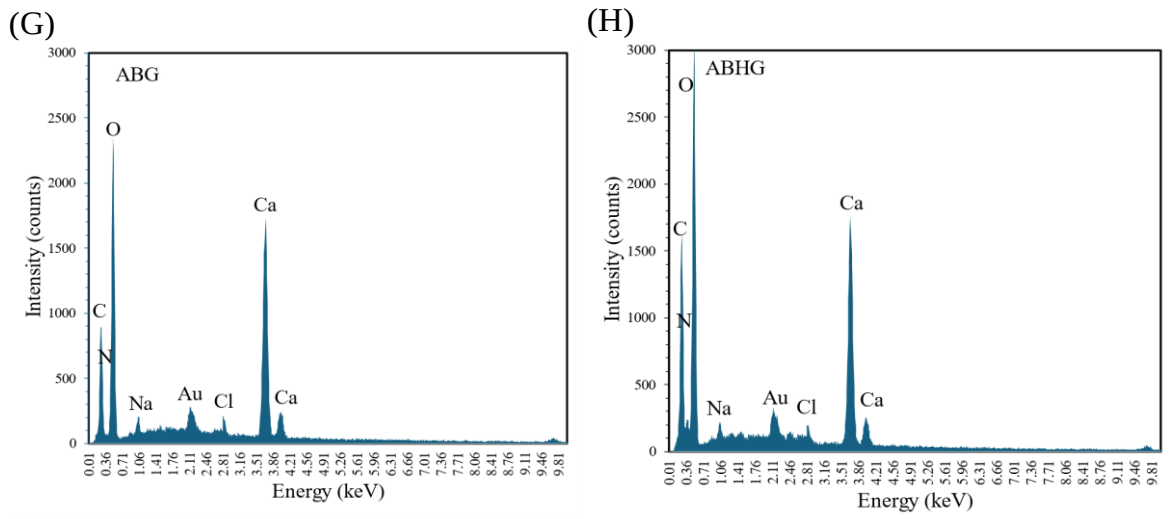

Figure 7 (Cont.) EDS spectrum of (A)control film and the alginate-based composite films: (B) AB, (C) AG, (D) AH, (E) AHB, (F) AHG, (G) ABG and (H) ABHG.

Across all samples, the main peaks consistently observed are for oxygen (O), carbon (C), calcium (Ca), sodium (Na), and chlorine (Cl). These elements form the baseline composition. Oxygen and carbon dominate the spectrum due to the organic matrix of sodium alginate and other carbon-based additives. Calcium is particularly prominent, as it is used for crosslinking the alginate through calcium chloride ($CaCl_2$). Sodium and chlorine likely originate from the alginate and $CaCl_2$, respectively. When comparing the control film to the other modified films, the elemental distribution remains largely consistent, but with subtle variations in intensity. The control film shows clear peaks for O, C, Na, Cl, and Ca, representing a typical alginate matrix. In the AB and AG films, the spectra are quite similar to the control, with some variation in the carbon and calcium peak intensities. Notably, the AG and AHG films display slight nitrogen (N) peaks, indicating the incorporation of nitrogen-rich g-C_3N_4 nanosheets. The AH and AHB films, which incorporate herbal extracts, show slightly higher carbon signals, suggesting an increase in organic content due to phytochemicals. AHG and ABHG films, which combine herbal extracts and g-C_3N_4, exhibit characteristics of both additives: elevated carbon from the herbal components and detectable nitrogen from g-C_3N_4. These composite films maintain a strong calcium signal, indicating stable crosslinking despite the presence of additional materials. In summary, the EDS spectra confirm the successful incorporation of various additives into the alginate film matrix. Herbal extracts contribute to higher carbon content, while g-C_3N_4 introduces nitrogen. The consistent presence of calcium across all spectra affirms the integrity of the crosslinked structure. These compositional differences correlate with the intended functional enhancements of each film type.

The water swelling values of the composite alginate films are summarised in Table 2. The control film exhibited the highest water swelling values, indicating that alginate films allowed the greatest diffusion of water molecules into their structure. This corresponded with the lowest contact angle compared to alginate films supplemented with nano-biochar, g-C_3N_4, and herbal extracts.

Therefore, it can be concluded that the control film illustrates the surface condition, displaying the lowest hydrophobicity. In contrast, the alginate film enhanced with nano-biochar, *A. paniculata* extract, and g-C_3N_4 exhibited the highest contact angle, indicating a hydrophobic surface. This ABHG composite film demonstrates superior hydrophobicity, corresponding to minimal water swelling. This suggests that this type of film is most effective at resisting water penetration. The increased hydrophobicity is attributed to g-C_3N_4, a material known for its surface hydrophobicity. Thus, the inclusion of g-C_3N_4 in the alginate film significantly enhances its hydrophobic property [25,26]. In addition, the incorporation of biochar into alginate films led to a decrease in surface energy values. Papadopoulou K. et al. reported that adding biochar to PLA increases the contact angle [27]. This effect is likely due to the pyrolysis process used in biochar production, which removes hydrophilic functional groups, thereby enhancing the material's hydrophobicity.

The experimental results demonstrated that the film containing *A. paniculata* herbal extract exhibited more than double the efficiency in inhibiting oxidation reactions compared to the film without the extract. This enhanced performance is attributed to the presence of flavonoid compounds in the *A. paniculata* extract, which effectively scavenges free radicals and resists oxidation reactions [28]. The chemical structure of flavonoids includes hydroxyl groups, unsaturated 2–3 conjugated bonds, a 4-oxo function, and carbohydrate moieties. The hydroxyl groups on the flavonoid rings donate electrons to free radicals such as hydroxyl, peroxyl, and peroxynitrite. This electron transfer stabilises these radicals and effectively reduces oxidation reactions [29]. In addition, many studies have also shown that *A. paniculata* extract is effective at inhibiting pathogenic microorganisms [30].

Table 2 Swelling, contact angle, and antioxidant of control film and alginate-based composite films.

Sample	Swelling (%)	Contact angle (Degree)	Antioxidant (%)
Control film	13.31 ± 0.52	25.81 ± 1.58	3.22 ± 0.03
AB	6.49 ± 0.20	30.13 ± 1.34	3.02 ± 0.08
AG	3.51 ± 0.23	31.35 ± 1.24	6.05 ± 0.18
AH	8.83 ± 0.18	28.30 ± 1.18	13.26 ± 0.26
AHB	4.20 ± 0.14	30.58 ± 1.39	12.20 ± 0.38
AHG	4.07 ± 0.24	36.36 ± 1.73	14.11 ± 0.89
ABG	3.35 ± 0.10	42.45 ± 0.83	5.28 ± 0.51
ABHG	1.21 ± 0.18	45.58 ± 1.57	13.32 ± 0.32

Although the AHG film demonstrated the highest antioxidant activity (14.11%), effective active packaging must not only inhibit oxidation reactions but also prevent moisture penetration, which can lead to mould growth on food. The moisture barrier property of a material is closely linked to its surface characteristics, with a more hydrophobic surface offering better moisture resistance. Despite its high antioxidant activity, contact angle measurements revealed that the AHG film was less hydrophobic than the ABHG film. This finding aligns with the film's water swelling behaviour, as ABHG exhibited the lowest swelling value, confirming its superior ability to prevent moisture transmission.

Overall, the chemical bond structure study revealed that the addition of biochar, *A. paniculata* extracts, and g-C_3N_4 nanosheets to the film did not create a new chemical structure. As a result, each component retained its distinct properties. Consequently, combining plant extracts with g-C_3N_4 enhances the potential to inhibit microorganisms. Furthermore, the incorporation of biochar into the composite films significantly enhanced their mechanical properties. Therefore, the ABHG alginate-based film with high antioxidant activity and hydrophobic property can be an efficient material for food packaging applications.

4. Conclusion

The integration of biochar, *A. paniculata* extract, and g-C_3N_4 nanosheets into sodium alginate films offers a promising approach to developing sustainable food packaging materials. The antimicrobial effectiveness of g-C_3N_4 nanosheets was evaluated using the poison food technique, demonstrating a significant antifungal activity against Fusarium sp. with a 21.12% inhibition rate at 1.0% concentration, surpassing the performance of the positive control, Metalaxyl. This result suggests that g-C_3N_4's unique two-dimensional structure, along with its potential to disrupt microbial cells, contributes to its antifungal properties. The incorporation of g-C_3N_4 into alginate films enhanced their properties, as evidenced by the addition of new chemical peaks in FTIR spectra confirming its successful integration. The mechanical analysis revealed that the biochar-infused alginate composite films exhibited enhanced rigidity, while the films containing *A. paniculata* extract displayed improved elongation but reduced modulus. Surface morphology analysis showed that g-C_3N_4 aggregation caused noticeable changes in the surface structure of the films, indicating a substantial impact on the film's texture. The addition of biochar and herbal extracts had lesser effects on surface roughness. The films incorporating g-C_3N_4 and biochar exhibited improved hydrophobicity, with reduced water swelling and higher contact angles compared to the control film. The alginate film with *A. paniculata* extract showed superior antioxidant activity, making it highly effective in inhibiting oxidation reactions. Overall, the alginate-based composite films demonstrated enhanced mechanical, antimicrobial, and antioxidant properties, making them promising candidates for food packaging applications where protection against both microbial contamination and oxidation is essential.

5. Acknowledgments

This research project was supported by Kasetsart University Kamphaeng Saen campus (KPS-RDI 2023-001), Research Promotion and Technology Transfer Center (RPTTC) and Department of Physical and Material Sciences, Faculty of Liberal Arts and Science.

6. Conflict of Interests

The authors declare no conflict of interest.

7. References

[1] Pilapitiya PGCNT, Ratnayake AS. The world of plastic waste: A review. Clean Mater. 2024;11:100-220.

[2] Radhika P, Lakshmi KR. Antimicrobial activity of the chloroform extracts of the root and the stem of *Andrographis paniculata* nees. Int Res J Microbiol. 2010;1(2):37–39.

[3] Shah R, Eldridge D, Palombo E, Harding I. Lipid nanoparticles: Production, characterization and stability. Springer Publ. 2015;3:107-111.

[4] Jaiyesimi KF, Agunbiade OS, Ajiboye BO, Afolabi OB. Polyphenolic-rich extracts of *Andrographis paniculata* mitigate hyperglycemia via attenuating β-cell dysfunction, pro-inflammatory cytokines and oxidative stress in alloxan-induced diabetic wistar albino rat. JDMDC. 2020;19(2):1543–1556.

[5] Saha P, Rahman FI, Hussain F, Rahman SMA, Rahman MM. Antimicrobial diterpenes: Recent development from natural sources. Front Pharmacol. 2022;28:1-2.

[6] Miklasińska-Majdanik M, Kępa M, Wojtyczka R, Idzik D, Wąsik T. Phenolic compounds diminish antibiotic resistance of staphylococcus aureus clinical strains. Int J Environ Res Public Health. 2018;15(10):231-232.

[7] Panche AN, Diwan AD, Chandra SR. Flavonoids: An overview. J Nutr Sci. 2016;5(47):2-9.

[8] Bhattacharya T, Khan A, Ghosh T, Kim JT, Rhim JW. Advances and prospects for biochar utilization in food processing and packaging applications. SM&T. 2024;39:e00831.

[9] Kane S, Van Roijen E, Ryan C, Miller S. Reducing the environmental impacts of plastics while increasing strength: Biochar fillers in biodegradable, recycled, and fossil-fuel derived plastics. JCOMC.2022; 8:1002-1053.

[10] Zouari M, Devallance DB, Marrot L. Effect of biochar addition on mechanical properties, Thermal Stability, and water resistance of hemp-polylactic acid (PLA) composites. Mater. 2022;15(6):22-71.

[11] Muhammad, Javed M, Shahid S, Shariq M, Fadhali MM, Ali SF, et al. Synthesis and applications of graphitic carbon nitride (g-C3N4) based membranes for wastewater treatment: A critical review. Heliyon. 2023;9(1):e12685–12695.

[12] Li R, Ren Y, Zhao P, Wang J, Liu J, Zhang Y. Graphitic carbon nitride (g-C_3N_4) nanosheets functionalized composite membrane with self-cleaning and antibacterial performance. J Hazard Mater. 2019;365:606–614.

[13] W. Apriliyani M, Purwadi P, Manab A, W. Apriliyanti M, D. Ikhwan A. Characteristics of moisture content, swelling, opacity and transparency with addition chitosan as edible films/coating base on casein. Adv J Food Sci Technol. 2020;18(1): 9–14.

[14] Anbarteh R, Aftabi-Khadar M, Hosseini-Hosseinabad SM, Seza A, Rahmani Fard S, Minaeian S. Effect of synthesis strategies on morphology and antibacterial properties and photocatalytic activity of graphitic carbon nitride (g-C_3N_4). Biomed Mater. 2024; 20(1):15036–15046.

[15] Narkbuakaew T, Sujaridworakun P. Synthesis of Tri-S-Triazine Based g-C_3N_4 Photocatalyst for Cationic Rhodamine B Degradation under Visible Light. Top Catal. 2020; 63(11-14):1086–1096.

[16] Darkwah WK, Ao Y. Mini review the structure and properties (*Photocatalysis*), and preparation techniques of graphitic carbon nitride Nano-Based particle, and its applications. Nanoscale Res Lett. 2018;13(1):2-9.

[17] Oboh IO, Aluyor EO, T O K Audu. Second-order kinetic model for the adsorption of divalent metal ions on Sida acuta leaves. IJPS. 2013; 8(34):1722–1728.

[18] Pattanasiri B, Sangjan S. Graphitic Carbon Nitride (g-C_3N_4) microrods and nanosheets photocatalysts immobilized on water hyacinth cellulose sponge for photodegradation. KEM. 2024;974:47–55.

[19] Erhonyota C, Edo GI, Onoharigho FO. Comparison of poison plate and agar well diffusion method determining the antifungal activity of protein fractions. Acta Ecol Sin. 2022;43(4):10-16.

[20] Kong X, Liu X, Zheng Y, Chu PK, Zhang Y, Wu S. Graphitic carbon nitride-based materials for photocatalytic antibacterial application. Mater Sci Eng R Rep. 2021;145:100610–100620.

[21] Wu M, Feng Q, Sun X, Wang H, Gielen G, Wu W. Rice (*Oryza sativa L*) plantation affects the stability of biochar in paddy soil. Scientific Reports. 2015;5(1):1-5.

[22] Sangeetha S, Archit R, Velu A.S. Phytochemical Testing, antioxidant activity, HPTLC and FTIR analysis of antidiabetic plants nigella sativa, *Eugenia jambolana*, *Andrographis paniculata* and *Gymnema sylvestre*. Res J Biotech. 2014;9:65-72.

[23] Wang H, Chen X, Wen Y, Li D, Sun X, Liu Z, et al. A study the correlation between the oxidation degree of oxidized sodium alginate Its degradability and gelation. Polymers. 2022;14(9):16-79.

[24] Abdel Aziz MS, Salama HE. Developing multifunctional edible coatings based on alginate for active food packaging. Int J Biol Macromol. 2021;190:837–844.

[25] Li Z, Meng X, Zhang Z. An effective approach to improve the photocatalytic activity of graphitic carbon nitride via hydroxyl surface modification. Catalysts. 2018;9(1):17–27.

[26] Li L, Zhang Y, Shi Y, Guo F, Yang X, Shi W. A hydrophobic high-crystalline g-C3N4/epoxy resin composite coating with excellent durability and stability for long-term corrosion resistance. Mater Today Commun. 2023;35:1056-1092.

[27] Papadopoulou K, Klonos PA, Kyritsis A, Tarani E, Chrissafis K, Mašek O, Synthesis and characterization of PLA/biochar bio-composites containing different biochar types and content. Polymers. 2025;17(3):26-33.

[28] Haque Md.E., Jahan I.A., Hossain H, Ethane N.J., Sarkar R. P, Moeiz S.Md.I. Comparative studies on antioxidant potential of *Andrographis Paniculata* grown in different places of Bangladesh. Int J Pharm Phytopharmacol Res. 2013;2(4):252-258.

[29] Heim KE, Tagliaferro AR, Bobilya DJ. Flavonoid antioxidants: Chemistry, metabolism and structure-activity relationships. JNB. 2002;13(10):572–584.

[30] Hossain S, Urbi Z, Karuniawati H, Mohiuddin RB, Moh Qrimida A, Allzrag AMM, Ming LC, Pagano E, Capasso R. *Andrographis paniculata* (Burm. f.) Wall. ex Nees: An updated review of phytochemistry, antimicrobial pharmacology, and clinical safety and efficacy. Life (Basel). 2021;11(4):34-38.